Electrochimica Acta 286 (2018) 14–21

Contents lists available at ScienceDirect

Electrochimica Acta

journal homepage: www.elsevier.com/locate/electacta

Low crystalline 2D CoS_x derived from cobalt carbonate hydroxide by sulfidation at room temperature for supercapacitor

J.P. Cheng [a, *], W.Q. Chen [a], S.Q. Gao [a], S.H. Guo [a, b], F. Liu [a]

[a] State Key Laboratory of Silicon Materials, School of Materials Science and Engineering, Key Laboratory of Advanced Materials and Applications for Batteries of Zhejiang Province, Zhejiang University, Hangzhou, 310027, China
[b] Center for High Pressure Science and Technology Advanced Research (HPSTAR), Shanghai, 201203, China

ARTICLE INFO

Article history:
Received 18 June 2018
Received in revised form
30 July 2018
Accepted 8 August 2018
Available online 9 August 2018

Keywords:
Cobalt sulfide
Phase transition
Electrode materials
Supercapacitor

ABSTRACT

Low crystalline CoS_x was fabricated by anion-exchange of 2-dimensional (2D) cobalt carbonate hydroxide (CoCH) using aqueous sodium sulfide solution at room temperature. It was proved that single crystalline CoCH nanoplates would transform into porous 2D CoS_x with low crystallinity after the anion-exchange. When they were used as electrode materials for supercapacitor, the 2D CoS_x material had a much higher specific capacitance than its precursor due to their different compositions and electroconductivities. CoS_x had a high specific capacitance of 863 F g^{-1} at 1 A g^{-1} and a good stability during long time charge-discharge processes, about 64.7% of initial capacitance retention after 10000 cycles. Asymmetric hybrid devices using 2D CoS_x as positive electrode and activated carbon as negative electrode were assembled, and the capacitor devices were able to achieve a high energy density of 33.56 Wh kg^{-1} at the power density of 400 W kg^{-1}. The high performances of the porous CoS_x make it a promising electrode material for energy storage.

1. Introduction

With the high-speed development of the society, renewable energy resources and energy storage devices have received much research attention in the world. The electrochemical storage devices including Li-ion batteries and supercapacitors (SC) are applied widely in many fields, such as portable devices, electric vehicles, *etc* [1]. The electrode materials are the most important factor for the performance of these energy storage devices [2,3]. Compared with Li-ion batteries, SCs are of higher power density, longer lifespan and faster charge/discharge process. However, the energy density of SCs is still limited. Thus, there were many previous reports which focused on the improvement of electrode materials for SCs [4–6]. In addition to carbon materials, battery-like electrode materials including transition metal oxides/hydroxides [3,7,8], sulfides [9,10] and their composites [11,12] have been deeply researched as novel electrode materials.

It is demonstrated by previous reports that transition metal sulfides have emerged as one of prominent candidates for SCs due to their high electroconductivity and rich redox chemistry [9,13–15]. $NiCo_2S_4$ and its composites have drawn much attention from researchers so far [16–19]. In general, the electrochemical performances of metal sulfides are strongly dependent on their composition and microstructure/morphology [20]. Among them, cobalt sulfides (CoS_x) have been also researched as electrode materials for SCs by Faradaic reaction due to its multiple phases and convenient synthesis. Recently, different morphologies of CoS_x materials such as hierarchical structures [21–23], nanowires [24–26], nanotubes [27], hollow structures [28,29], 2-dimensional (2D) nanosheets [30,31] and composites [32–35] have been reported as electrode materials for SCs. Until now, the research of 2D CoS_x for SCs still has many limitations. Rakhi et al. reported that Co_9S_8 nanoflakes nucleated over carbon fibers showed a high specific capacitance of 1056 F g^{-1} at 5 mV s^{-1} [32]. Han and co-workers prepared Co_9S_8 nanosheet arrays on Ni foam which exhibited a high specific capacitance of 1098.8 F g^{-1} at 0.5 A g^{-1} [31]. Above reports are related to 2D Co_9S_8 films grown on current collectors for SCs. However, the research on powder 2D CoS_x is still very limited.

In this work, 2D CoS_x powder with low crystallinity was fabricated by simple anion exchange of cobalt carbonate hydroxide using Na_2S solution at room temperature. The microstructure and electrochemical performance of 2D CoS_x were investigated. The 2D

* Corresponding author.
E-mail address: chengjp@zju.edu.cn (J.P. Cheng).

https://doi.org/10.1016/j.electacta.2018.08.035
0013-4686/

CoS_x material had the similar morphology to its precursor and showed a high specific capacitance of 863 F g^{-1} at 1 A g^{-1} as well as a good cycling stability. When it was used as a positive electrode and combined with activated carbon as a negative electrode to assemble a hybrid capacitor, the capacitor could deliver a high energy density of 33.56 Wh Kg^{-1} at 400 W kg^{-1} in a voltage window of 1.6 V, showing its great potential for energy storage.

2. Experimental

2.1. Materials

Cobalt acetate, hexamethylene tetramine (HMT), sodium sulfide, and KOH were used as received without further purification. Deionized water was used in all of the experiments.

2.2. Preparation of 2D CoS_x

In a typical procedure for the synthesis of 2D cobalt carbonate hydroxide, 2.5 mmol cobalt acetate and 7.5 mmol HMT were dissolved in 16 mL water. The obtained solution was transferred into a Teflon-lined stainless-steel autoclave with a total volume of 20 mL. The autoclave was sealed and maintained at 210 °C for 2 h reaction. Thereafter, the solution was cooled down to room temperature and filtered, and the obtained cobalt carbonate hydroxide (CoCH) with pink color was rinsed by water several times to remove the residual reactant. To prepare 2D CoS_x, the CoCH powder was anion exchanged by Na_2S solution. The method was similar to our previous report [9]. 20 mL saturated Na_2S solution was dropwise added into the suspension of 0.2 g CoCH in 50 mL water at room temperature under a nitrogen atmosphere in 1 h. After the suspension was stirred for 3 more hours at room temperature, black CoS_x product was filtered and washed by adequate water, and then dried at 80 °C.

2.3. Structure and electrochemical measurements

The phase of cobalt compounds was characterized by a powder X-ray diffractometer (XRD, PANalytical, Empyrean) using Cu-Kα irradiation (λ = 1.5406 Å) from 10° to 80°. A scanning electron microscope (SEM, Hitachi S-4800) and a transmission electron microscope (TEM, Philips-CM200) were used to characterize their morphologies and microstructures. The chemical analysis of materials was carried out by X-ray photoelectron spectroscopy (XPS, Shimadzu, AXIS Supra). Fourier transformed infrared (FTIR) spectrum was measured by a Bruker spectrometer (TENSOR 27).

The electrochemical performance of the materials was measured under a three-electrode system in 2 M KOH aqueous solution as electrolyte. The electrode was prepared by painting 80 wt% active material onto the surface of Ni foam using 10 wt% acetylene black and 10 wt% PVDF as conductive addition and polymer binder, respectively, and the mass loading of active material on each electrode was about 5 mg. The specific capacitance (C_s, in F g^{-1}) is calculated by the following equation,

$$C_s = I \times t/(m \times \Delta V) \quad (1)$$

wherein I (A), t (s), m (g), ΔV (V) represent the discharge current, discharge time, mass of active material and potential window, respectively.

Hybrid capacitors with 2D CoS_x as positive electrode and activated carbon (AC) as negative electrode, a piece of cellulose paper as the separator were assembled to evaluate their potential application. The electrochemical properties of the hybrid capacitors were measured in a two-electrode system in 2 M KOH. The energy density (E, Wh Kg^{-1}) and power density (P, W Kg^{-1}) of the hybrid capacitors can be calculated according to the following two equations,

$$E = \frac{1}{7.2} C \times \Delta V^2 \quad (2)$$

$$P = E/\Delta t \quad (3)$$

where C (F g^{-1}), ΔV (V), Δt (s) represent the specific capacitance of hybrid capacitor, potential window and discharge time, respectively.

3. Results and discussions

3.1. Structure and morphology characterization

The XRD patterns of CoCH precursor and CoS_x are shown in Fig. 1. In Fig. 1a, the high intensity of XRD peaks implies the crystalline nature of CoCH. The peaks at 14.65°, 17.44° and 24.03° are corresponding to the (020), (120) and (220) planes of cobalt carbonate hydroxide (PDF No. 29-1416). In addition to the peaks from CoCH, some diffraction peaks from cobalt carbonate (PDF No. 11-0692) can be also observed. We found that the reaction temperature was a rather important factor for the phase of the final product. Below 120 °C, the main product was alpha cobalt hydroxide [36,37].

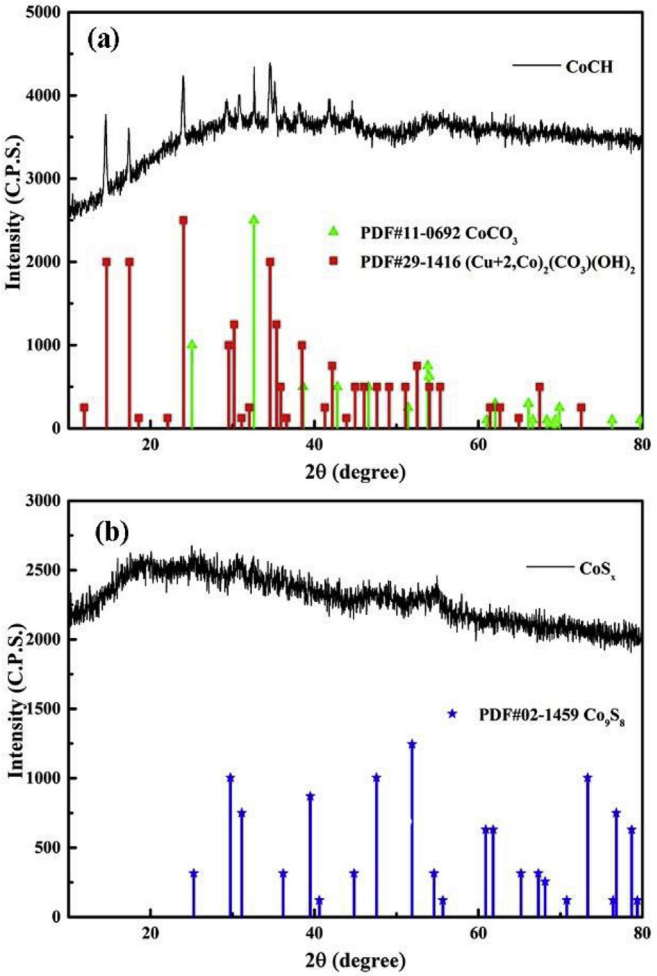

Fig. 1. XRD patterns of CoCH (a) and CoS_x (b).

From 150 to 180 °C, cobalt carbonate could be obtained. When the temperature was above 210 °C, cobalt carbonate hydroxide with a high yield was thus fabricated. When CoCH was reacted with saturated Na_2S solution at room temperature, its pink suspension turned to be black rapidly, implying an anion-exchange reaction happened to form CoS_x. The reaction mechanism is similar to our previous report [9]. The diffraction pattern of the CoS_x product is exhibited in Fig. 1b, where only two small weak peaks at about 30.67° and 54.9° can be observed. It proves the low-crystallinity of the CoS_x product [38]. Even it was heated at 300 °C for 2 h in a nitrogen atmosphere, it still had rather poor crystallinity, as shown in Fig. S1.

The typical SEM images of CoCH and CoS_x are shown in Fig. 2 to investigate their morphologies and structures. In Fig. 2a, we can see that the morphology of CoCH product shows the clusters composed of nanoplates and that these nanoplates are randomly interconnected with each other. A high magnified image in Fig. 2b exhibits the typical lamellar nature of the nanoplates with a thickness about 50 nm. It should be mentioned that the layered structure can be well reserved after anion-exchange, as shown in Fig. 2c and d. It means that the phase transition from cobalt carbonate hydroxide to CoS_x has few effects on their general morphology.

The microstructure of the two samples was further observed by TEM, as displayed in Fig. 3. As shown in Fig. 3a, CoCH exhibits plate-like morphology, which is consistent with SEM images. These nanoplates have sharp and clear edges due to its single crystallinity. The homogenous image contrast proves their uniform thickness. The selected-area electron diffraction (SAED) pattern of a nanoplate in Fig. 3b confirms its single-crystalline nature and layered structure. The structure of CoS_x nanoplates was also elucidated by TEM observation, as shown in Fig. 3c-e. The CoS_x nanoplates exhibit a porous plate-like structure under a low magnification in Fig. 3c, which is different from its precursor. A lot of small pores are distributed in the whole block from the image contrast. A high-magnified TEM in Fig. 3d shows that many small grains can be found in the frame of the nanoplate. A high-resolution TEM image in Fig. 3e also proves its low crystallinity and shows the size of grains about 20 nm. Compared with its precursor, its implies that the anion-exchange reaction causes to the formation of a porous 2D CoS_x structure. From the SAED pattern in the inset of Fig. 3e, the crystallinity of CoS_x is very poor, even to be amorphous, which is in good accordance with the XRD analysis. Based on the above results, porous CoS_x nanoplates can be easily synthesized by anion-exchange of 2D CoCH at room temperature [9]. The porous structure of 2D CoS_x can greatly increase the quantity of electroactive sites and facilitate the transport of aqueous electrolyte, which is significant to enhance the electrochemical performance of electrode materials for the energy storage.

The FTIR spectra of CoCH and CoS_x are both shown in Fig. 4a. For sample CoCH, the strong peak at about 3505 cm^{-1} is assigned to the stretching vibration of O—H groups of molecular water. The shoulder vibration at around 3382 cm^{-1} is attributed to the O—H groups interacting with carbonate anions. The peak at 1633 cm^{-1} is due to the bending mode from water [39]. These bands from carbonate anions are clearly presented to prove its existence. The characteristic peaks of carbonate anions were located at 1557, 1344, 1069 and 836 cm^{-1}, corresponding to the $\nu(OCO_2)$, $\nu(CO_3)$, $\nu(C{=}O)$ and $\delta(CO_3)$, respectively [40]. The peak observed at 970 cm^{-1} is a characteristic bending mode of Co—OH. For CoS_x, the broad peak at 3381 cm^{-1} is corresponding to O—H group of water. The intensity of other bands related to carbonate anions and water is decreased due to the phase transition. However, a strong peak at about 1095 cm^{-1} is assigned to Co═S stretching vibration originating from the presence of cobalt sulfide [31]. The strong band at 631 cm^{-1} can be

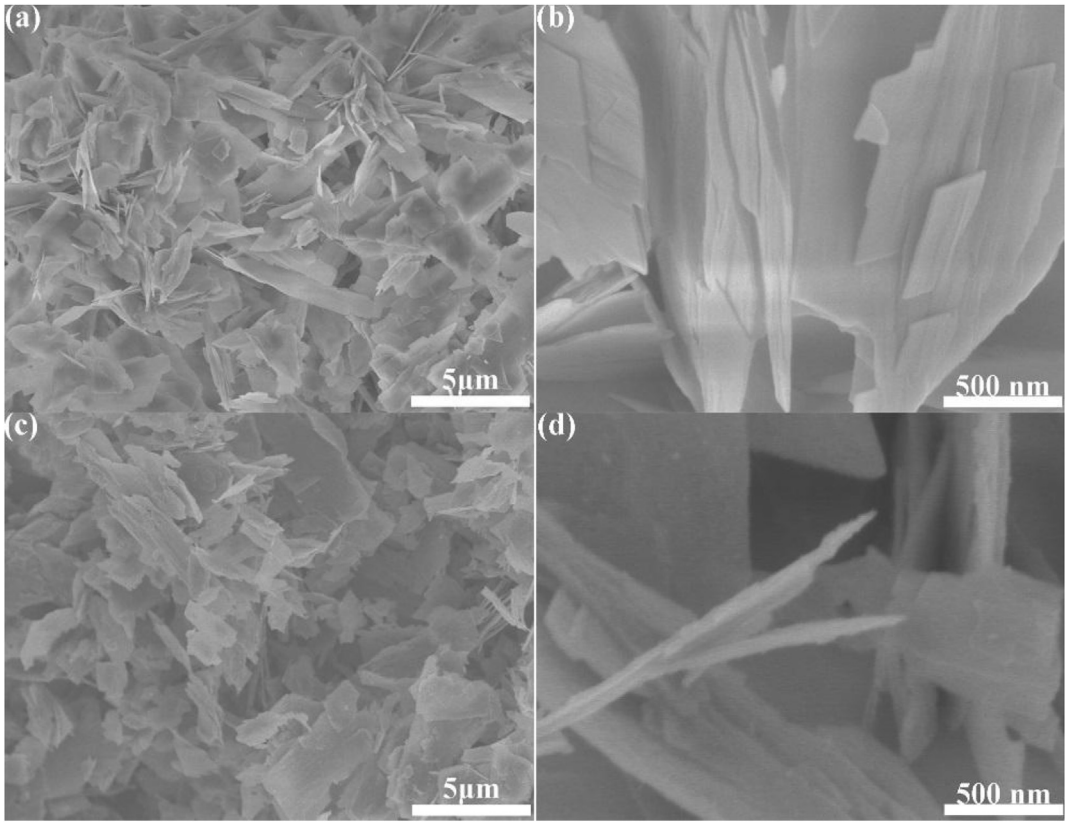

Fig. 2. SEM images of (a,b) 2D CoCH and (c,d) 2D CoS_x at different magnifications.

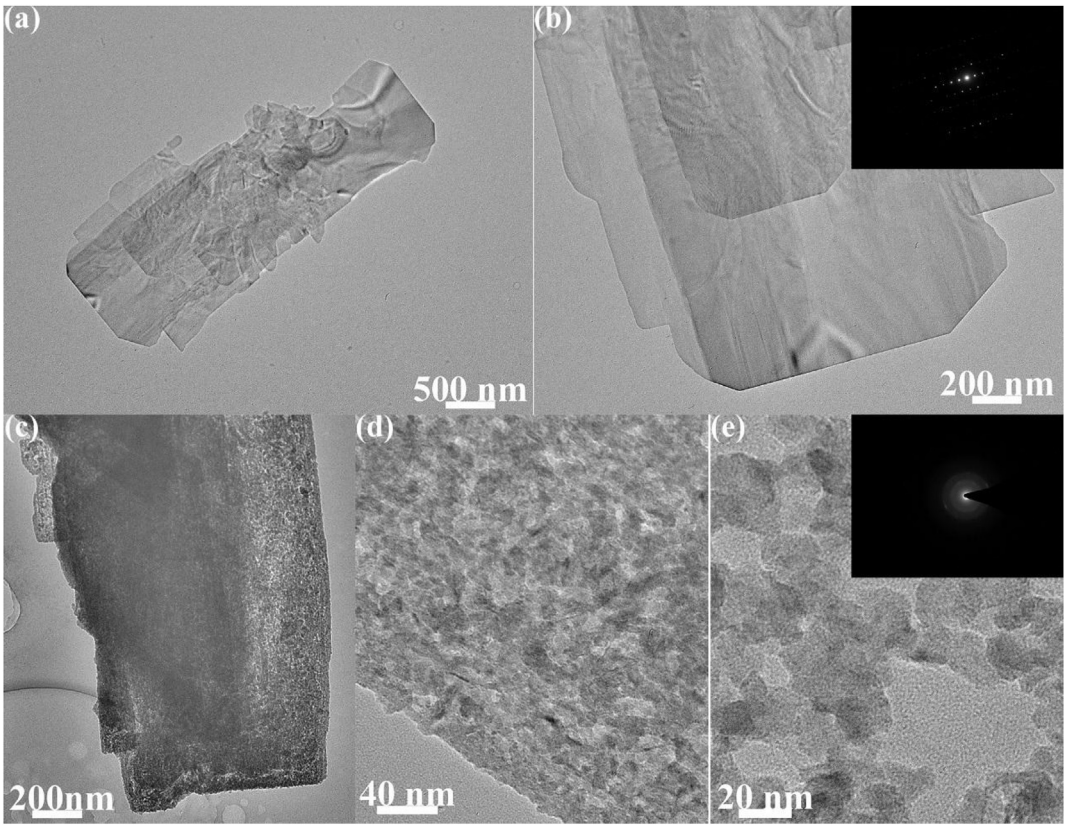

Fig. 3. TEM images of (a,b) 2D CoCH and (c,d,e) porous CoS_x at different magnifications, the inset showing their SAED patterns.

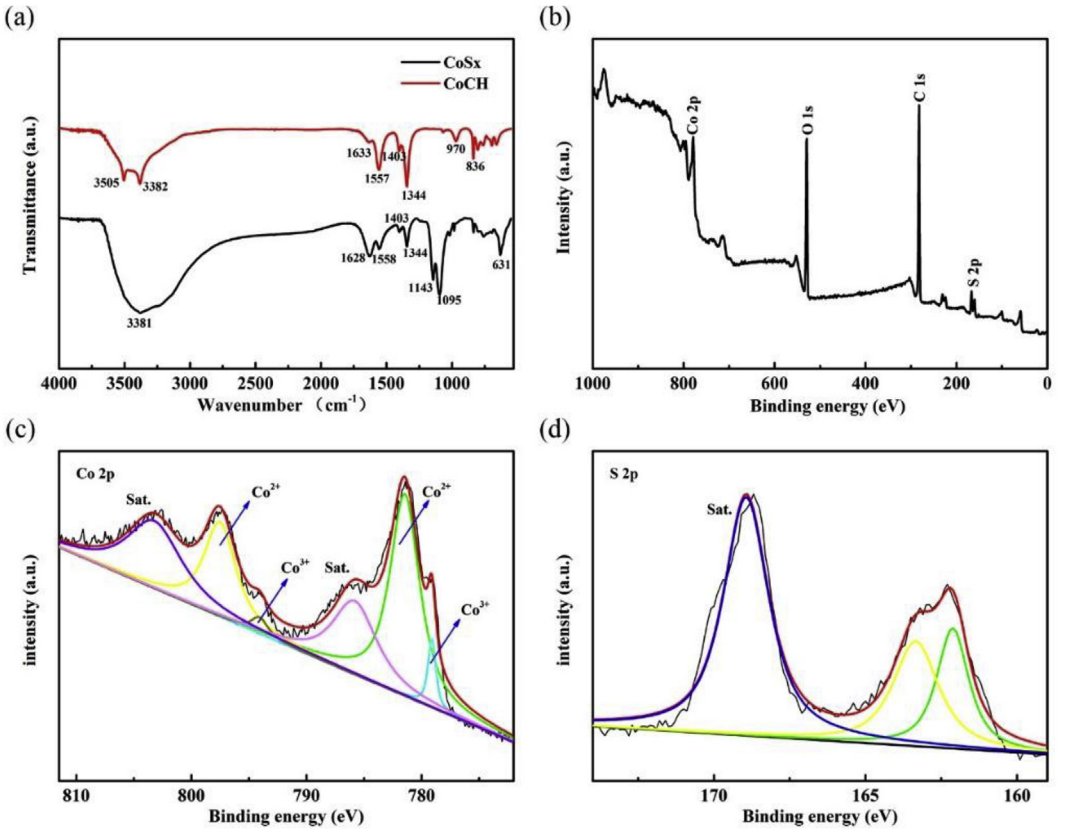

Fig. 4. (a) FTIR spectra of CoCH and CoS_x, and (b–d) XPS spectra of CoS_x.

also attributed to the Co–S vibration modes in the CoS_x [41].

The chemical composition of CoS_x nanoplates was investigated by XPS analysis, as shown in Fig. 4b-d. The wide spectrum in Fig. 4b suggests the existence of Co, S, O and C elements. O and C are present due to the exposure to air. The high-resolution Co 2p spectrum in Fig. 4c exhibits two spin-orbit doublets $2p_{1/2}$ and $2p_{3/2}$, the peaks at 797.6 eV and 781.5 eV are the characteristic of Co^{2+}, while the peaks at 794.2 eV and 779.1 eV are from Co^{3+}, implying the coexistence of Co^{2+} and Co^{3+} in the CoS_x. Fig. 4d is the S 2p spectrum. Two peaks of $2p_{1/2}$ and $2p_{3/2}$ can be observed at the binding energies of 163.4 eV and 162.1 eV, respectively, which is typical coordination of sulfur ions with metal ions [27]. The additional satellite peak at about 169 eV corresponds to the S^{4+} species in sulfate groups [31]. Thus, FTIR and XPS results both prove the successful fabrication of cobalt sulfide.

3.2. Electrochemical properties

The electrochemical performances of CoS_x and its precursor were investigated and compared in 2 M KOH. The cyclic voltammetry (CV) curves of CoS_x are presented in Fig. 5a at different scan rates from 5 to 50 mV s^{-1} in a potential window of 0.5 V. Each curve shows a pair of redox peaks, an anodic peak at about 0.21 V and a cathodic peak at around 0.35 V, indicating the battery-like behavior. The surface Faradic redox reaction can be described as Eq. (4) [42]. The shape of the CV curve changes slightly with the increasing scan rate, implying that its unique structure can endure fast redox reactions. The CV curves of CoS_x and CoCH at 5 mV s^{-1} are both exhibited in Fig. 5b, and the curve of CoS_x has a much larger enclosed area than that of CoCH, implying its higher specific capacitance than that of CoCH.

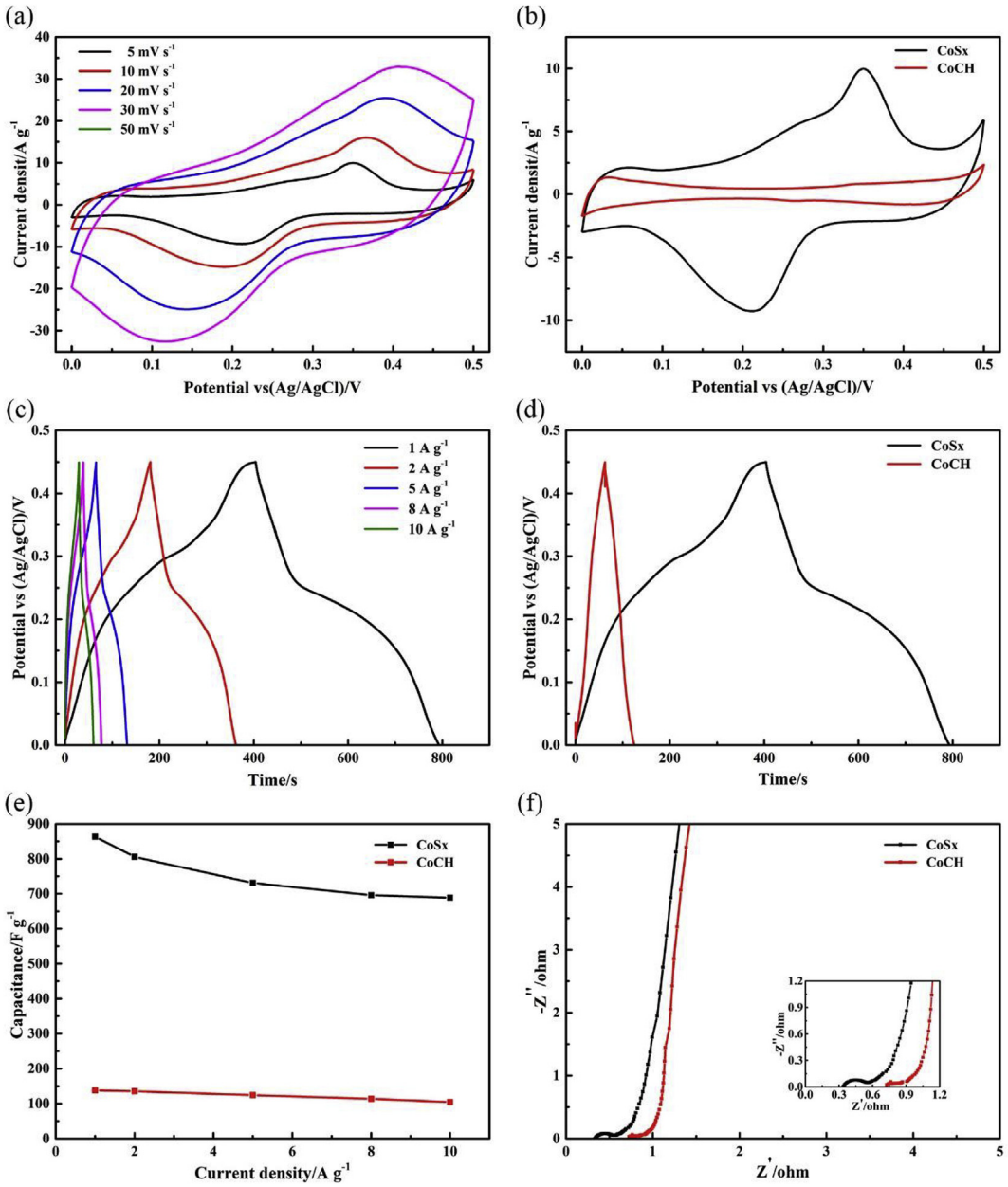

Fig. 5. The electrochemical performances of CoS_x and CoCH. (a) CV curves of CoS_x at different scan rates, (b) CV curves of CoS_x and CoCH at 5 mV s^{-1}, (c) GCD curves of CoS_x at different current densities, (d) GCD curves of CoS_x and CoCH at 1 A g^{-1}, (e) the dependence of specific capacitance on the current density and (f) EIS plots of CoS_x and CoCH electrodes.

$$CoS_x + OH^- \leftrightarrow CoS_xOH + e^- \quad (4)$$

The galvanostatic charge-discharge (GCD) curves of CoS_x at different current densities are shown in Fig. 5c, showing two small plateau regions due to the redox reactions. The symmetric shape and the equal charge-discharge time prove its high Coulombic efficiency. The calculated specific capacitance values for CoS_x are 863, 805, 731, 695 and 689 F g^{-1} at 1, 2, 5, 8 and 10 A g^{-1} from the discharge curves according to Eq. (1), respectively. For a straightforward comparison, the GCD curves of CoS_x and CoCH at 1 A g^{-1} are shown in Fig. 5d, in which the charge and discharge time of CoS_x electrode is much longer than that of CoCH at the same current density. It is clearly demonstrated that CoS_x has a much higher specific capacitance than CoCH. The detailed CV and GCD curves of CoCH are exhibited in Fig. S2. The dependence of specific capacitance on the current density of the two electrode materials are compared in Fig. 5e, in which CoS_x delivers higher specific capacitance than CoCH at any current density. CoCH has the specific capacitance less than 150 F g^{-1}. They have comparable rate capability, about 80% retainment of specific capacitance from 1 to 10 A g^{-1}.

The electrochemical impedance spectroscopy (EIS) is also measured, as shown in Fig. 5f, where the insert is a magnified image in high-frequency region. Each plot is composed of a semicircle in the high-frequency region and a straight line in the low-frequency region. As shown in the insert, the R_s value (the intercept on the real axis) of CoS_x electrode is only 0.33 Ω, which is much smaller than that of CoCH (0.73 Ω), indicating its higher electroconductivity. As an electrode material for practical application, its cycle stability is also a very crucial factor. In this work, the repeated charge and discharge measurement for 10000 cycles was conducted at 5 A g^{-1} to test the cycle stability of CoS_x and CoCH. As shown in Fig. S3 (a-b), the specific capacitance retention for CoCH and CoS_x is 95.6% and 64.7%, respectively. CoS_x electrode shows a worse stability than CoCH. It may be caused by the possible phase transition from metal sulfide to metal hydroxide during the long-time Faradic reaction in alkaline electrolyte due to the instability of the amorphous and porous structure [15]. A typical SEM image of the CoS_x electrode after test is shown in Fig. S4, where some hexagonal nanoplate are generated. It may be a clue to the formation metal hydroxide.

Previous reports demonstrated that amorphous $Ni(OH)_2$ [43] and MnO_2 [44] had improved capacitance and excellent rate capability due to the disorder structures. However, there are only a few reports on amorphous metal sulfides for SCs. Zhang et al. [45] designed double-shelled polyhedral nanocages consisting of ultrathin amorphous Ni_xS_y layer on the hollow CoS nanocages using a MOFs-engaged strategy for SCs. Zhai and co-workers [46] compared amorphous and crystalline CoS_2 for SCs application by experimental characterization and theoretical calculations. Amorphous CoS_2 had a lower band gap and higher main D-orbital peak than those of the crystalline [46]. In this work, CoS_x and its precursor both have 2D morphology. Metal sulfides usually have better electroconductivity than the corresponding metal carbonate hydroxides, thus resulting in faster electron transport behavior. A large quantity of electroactive sites can be obtained in a porous structure. Thus, CoS_x material has prominently enhanced electrochemical performances than CoCH.

The specific capacitance of low-crystalline CoS_x material in this work and those of other CoS_x compounds reported in the literature are listed in Table 1, in order to obtain a comparison of CoS_x materials. The CoS_x material in this work shows a higher specific capacitance than most of crystalline CoS materials. The 2D Co_9S_8 nanoarrays in Ref. [31] showed a higher value than this work, because the Co_9S_8 films on Ni foam were used as work electrodes directly.

3.3. Electrochemical performance of hybrid capacitors

In order to further explore the performance of CoS_x material for practical application, CoS_x//AC hybrid capacitor devices were assembled. A hybrid capacitor is an electrochemical cell, which presents the characteristic of a capacitor based on a capacitive electrode and a redox battery-type electrode [49]. In this work, CoS_x was selected as a positive electrode, and AC as a negative electrode. The CV curves of CoS_x and AC at 5 mV s^{-1} are exhibited in Fig. 6a, where AC and CoS_x have stable voltage windows between −1.2 and 0 V and from 0 to 0.5 V, respectively. Thus CoS_x// AC hybrid capacitor is expected to achieve a wide voltage window of 1.6 V. After the stored charges in both electrodes were balanced [9], the optimized mass ratio of CoS_x to AC was 1:1.6.

The performances of CoS_x//AC hybrid capacitors were measured in a two-electrode system in 2 M KOH solution. The CV curves of the hybrid capacitor are shown in Fig. 6b at the scan rates from 5 to 50 mV s^{-1} within a potential window of 1.6 V. The well reserved CV shapes at different scan rates prove the outstanding reversibility of the hybrid capacitor. The GCD curves in Fig. 6c are slightly nonlinear, showing its pseudocapacitive behavior. The specific capacitance by taking account of the total mass of the materials in both electrodes at different current densities is shown in the insert of Fig. 6d. The specific capacitance of the capacitor is calculated to be 94, 85, 77, 70 and 69 F g^{-1} at 0.5, 1, 2, 4 and 5 A g^{-1}, respectively.

The Ragone plot relative to the energy density and the corresponding power density is calculated from the discharge curves of a typical hybrid capacitor, as shown in Fig. 6d. It can achieve the highest energy density up to 33.56 Wh kg^{-1} at the power density of 400 W kg^{-1}, and the power density as high as 4000 W kg^{-1} at the energy density of 24.11 Wh kg^{-1}. The energy and power densities of the CoS_x//AC capacitor device is shown in Table S1 along with those of various CoS_x//AC devices reported in the literature. The highest energy density of this work is moderate among them. The high energy densities in Refs. [48] and [23] are derived from CoS_x@carbon composite and Co_9S_8 arrays grown on Ni foam, respectively. This inspires us that structural design and composite preparation are two potential strategies to further improve the performances of

Table 1
Comparison of specific capacitance of CoS_x electrode materials.

Materials	Electrolyte	Mass loading	Current density	Specific capacitance	Ref.
Crystalline CoS	3 M KOH	3 mg cm^{-2}	0.5 A g^{-1}	586 F g^{-1}	[34]
Crystalline CoS	6 M KOH	2.0–3.0 mg	1 A g^{-1}	586 F g^{-1}	[22]
Crystalline CoS	6 M KOH	12.5 mg	0.5 A g^{-1}	285 F g^{-1}	[24]
CoS_2 nanoparticles	6 M KOH	–	1 A g^{-1}	431 F g^{-1}	[47]
CoS_2 Nanowires @carbon cloth	6 M KOH	1.18 mg cm^{-2}	1 A g^{-1}	355 F g^{-1}	[25]
Co_9S_8 arrays@Ni foam	1 M KOH	2.8 mg cm^{-2}	1 A g^{-1}	954 F g^{-1}	[31]
CoS_2@thin carbon layer	2 M KOH	3 mg	1 A g^{-1}	750 F g^{-1}	[48]
2D CoS_x	2 M KOH	5 mg	1 A g^{-1}	863 F g^{-1}	This work

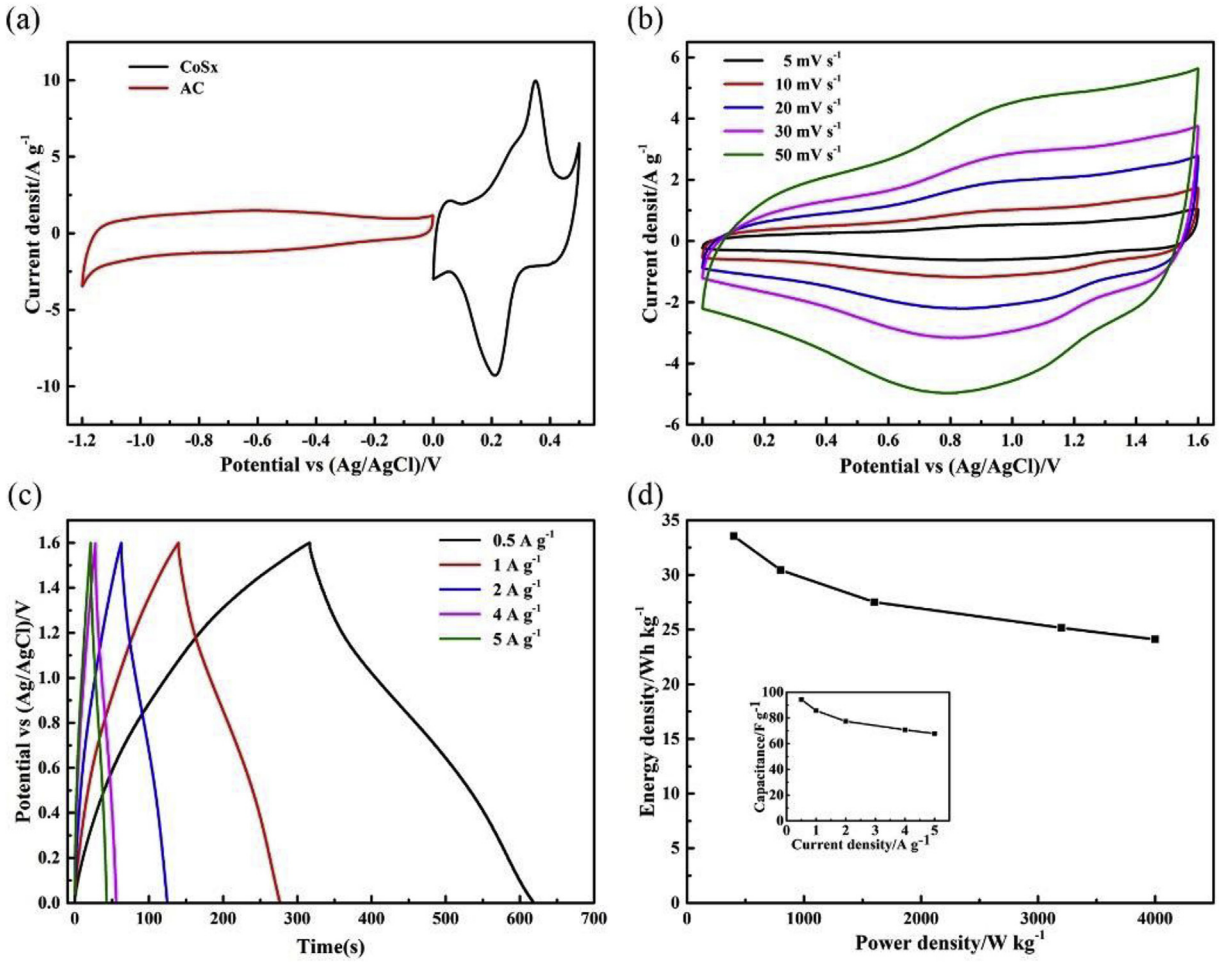

Fig. 6. (a) CV curves of CoS_x and AC at 5 mV s^{-1}, (b) CV curves of CoS_x//AC hybrid capacitor at different scan rates, (c) GCD curves of a hybrid capacitor at different current densities, and (d) Ragone plot of a CoS_x//AC hybrid capacitor, insert showing its specific capacitance at different current densities.

the 2D CoS_x materials.

To further demonstrate the performance of CoS_x//AC capacitors, it was measured for a long-time charge-discharge process. The relation of capacitance to cycle number is shown in Fig. S5. It shows about 31.25% capacity decline after 10000 successive cycles. Two capacitor devices could be connected in series for a higher operating potential. They were used to power a red LED lamp that could light above 3 V. The lamp connected to the two cells could shine for about 5 min, as shown in Fig. S6. Above results prove that the CoS_x// AC device is a promising electrochemical device for energy storage application.

4. Conclusions

Two-dimensional CoS_x nanoplates can be easily fabricated by anion-exchange of 2D CoCH by Na_2S aqueous solution at room temperature. The layered morphology of CoCH is well retained after the reaction. However, the CoS_x nanoplates are low crystalline, nearly amorphous, and have a porous structure, which are basically different from the precursor. The 2D CoS_x exhibits a remarkably higher specific capacitance than CoCH due to its unique structure and composition. CoS_x nanoplates and activated carbon can be assembled into hybrid capacitors. The CoS_x//AC hybrid capacitor has a high energy density and good cycling stability. The above results exhibit the potential applications of this low crystalline CoS_x material for energy storage.

Acknowledgement

This work was financially supported by Zhejiang Provincial Natural Science Foundation of China (No. LY18E020003).

Appendix A. Supplementary data

Supplementary data related to this article can be found at https://doi.org/10.1016/j.electacta.2018.08.035.

References

[1] U. Olsbye, S. Svelle, K.P. Lillerud, Z.H. Wei, Y.Y. Chen, J.F. Li, J.G. Wang, W.B. Fan, The formation and degradation of active species during methanol conversion over protonated zeotype catalysts, Chem. Soc. Rev. 44 (2015) 7155–7176.
[2] J. Yan, Q. Wang, T. Wei, Z. Fan, Supercapacitors: recent advances in design and fabrication of electrochemical supercapacitors with high energy densities, Adv. Energy Mater. 4 (2014), 1300816.
[3] J.P. Cheng, J. Zhang, F. Liu, Recent development of metal hydroxides as electrode material of electrochemical capacitors, RSC Adv. 4 (2014) 38893–38917.
[4] X. Li, B. Wei, Supercapacitors based on nanostructured carbon, Nano Energy 2 (2013) 159–173.
[5] A. González, E. Goikolea, J.A. Barrena, R. Mysyk, Review on supercapacitors: technologies and materials, Renew. Sustain. Energy Rev. 58 (2016) 1189–1206.
[6] D. Cericola, R. Kötz, Hybridization of rechargeable batteries and electrochemical capacitors: principles and limits, Electrochim. Acta 72 (2012) 1–17.
[7] M. Li, J.P. Cheng, F. Liu, X.B. Zhang, 3D-architectured nickel-cobalt-manganese layered double hydroxide/reduced graphene oxide composite for high-performance supercapacitor, Chem. Phys. Lett. 640 (2015) 5–10.

[8] X.L. Zhang, X. Han, X.X. Zhao, J. Qi, Q.X. Ma, K. Tao, L. Han, Construction of Ni-Co-Mn layered double hydroxide nanoflakes assembled hollow nanocages from bimetallic imidazolate frameworks for supercapacitors, Mater. Res. Bull. 106 (2018) 243–249.

[9] S. Guo, W. Chen, M. Li, J. Wang, F. Liu, J.P. Cheng, Effect of reaction temperature on the amorphous-crystalline transition of copper cobalt sulfide for supercapacitors, Electrochim. Acta 271 (2018) 498–506.

[10] G.C. Li, M.M. Liu, M.K. Wu, P.F. Li, Z.W. Zhou, S.R. Zhu, R. Liu, L. Han, MOF-derived self-sacrificing route to hollow NiS_2/ZnS nanospheres for high performance supercapacitors, RSC Adv. 6 (2016) 103517–103522.

[11] J. Fang, M. Li, Q. Li, W. Zhang, Q. Shou, F. Liu, X. Zhang, J. Cheng, Microwave-assisted synthesis of CoAl-layered double hydroxide/graphene oxide composite and its application in supercapacitors, Electrochim. Acta 85 (2012) 248–255.

[12] M. Li, J.P. Cheng, J. Wang, F. Liu, X.B. Zhang, The growth of nickel-manganese and cobalt-manganese layered double hydroxides on reduced graphene oxide for supercapacitor, Electrochim. Acta 206 (2016) 108–115.

[13] X. Rui, H. Tan, Q. Yan, Nanostructured metal sulfides for energy storage, Nanoscale 6 (2014) 9889–9924.

[14] G. Tang, L. Cao, P. Xiao, Y. Zhang, H. Liu, A novel high energy hybrid Li-ion capacitor with a three-dimensional hierarchical ternary nanostructure of hydrogen-treated TiO_2 nanoparticles/conductive polymer/carbon nanotubes anode and an activated carbon cathode, J. Power Sources 355 (2017) 1–7.

[15] J. Wang, K.Y. Ma, J. Zhang, F. Liu, J.P. Cheng, Template-free synthesis of hierarchical hollow NiSx microspheres for supercapacitor, J. Colloid Interface Sci. 507 (2017) 290–299.

[16] Z. Wu, X. Pu, X. Ji, Y. Zhu, M. Jing, Q. Chen, F. Jiao, High energy density asymmetric supercapacitors from mesoporous $NiCo_2S_4$ nanosheets, Electrochim. Acta 174 (2015) 238–245.

[17] C. Chen, M.K. Wu, K. Tao, J.J. Zhou, Y.L. Li, X. Han, L. Han, Formation of bimetallic metal-organic framework nanosheets and their derived proofs nickel-cobalt sulfides for supercapacitor, Dalton Trans. 47 (2018) 5639–5645.

[18] Q.D. Chen, J.K. Miao, L. Quan, D.P. Cai, H.B. Zhan, Bimetallic $CoNiS_x$ nanocrystallites embedded in nitrogen-doped carbon anchored on reduced graphene oxide for high-performance supercapacitor, Nanoscale 10 (2018) 4051–4060.

[19] K. Tao, X. Han, Q.X. Ma, L. Han, A metal-organic framework derived hierarchical nickel-cobalt sulfide nanosheet array on Ni foam with enhanced electrochemical performances for supercapacitors, Dalton Trans. 47 (2018) 3496–3502.

[20] H. Chen, J. Jiang, Y. Zhao, L. Zhang, D. Guo, D. Xia, One-pot synthesis of porous nickel cobalt sulphides: tuning the composition for superior pseudocapacitance, J. Mater. Chem. A 3 (2014) 428–437.

[21] K.J. Huang, J.Z. Zhang, G.W. Shi, Y.M. Liu, One-step hydrothermal synthesis of two-dimensional cobalt sulfide for high-performance supercapacitors, Mater. Lett. 131 (2014) 45–48.

[22] F. Luo, J. Li, H. Yuan, D. Xiao, Rapid synthesis of three-dimensional flower-like cobalt sulfide hierarchitectures by microwave assisted heating method for high-performance supercapacitors, Electrochim. Acta 123 (2014) 183–189.

[23] S. Zhang, C. Li, H. Xiao, G. Wei, Y. Zhou, Z. Wang, J. Zhang, C. An, Synthesis of 3D flower-like cobalt sulfide hierachitecture for high-performance electrochemical energy storage, J. Nanoparticle Res. 19 (2017) 202.

[24] J.M. Chiu, L.Y. Lin, P.H. Yeh, C.Y. Lai, K. Teng, C.C. Tu, S.S. Yang, J.F. Yu, Synthesizing highly conductive cobalt sulfide hydrangea macrophylla using long carbon-chain sulfur source for supercapacitors, RSC Adv. 5 (2015) 83383–83390.

[25] R. Ren, M.S. Faber, R. Dziedzic, Z. Wen, S. Jin, S. Mao, J. Chen, Metallic CoS_2 nanowire electrodes for high cycling performance supercapacitors, Nanotechnology 26 (2015), 494001.

[26] S.J. Bao, C.M. Li, C.X. Guo, Y. Qiao, Biomolecule-assisted synthesis of cobalt sulfide nanowires for application in supercapacitors, J. Power Sources 180 (2008) 676–681.

[27] D.B. Xiong, X.F. Li, Z.M. Bai, J.W. Li, Y. Han, D.J. Li, Vertically aligned Co_9S_8 nanotube arrays onto graphene papers as high-performance electrodes for supercapacitors, Chem. Eur. J. 24 (2018) 2339–2343.

[28] J. Wang, L. Li, X. Chen, Y. Lu, W. Yang, Monodisperse cobalt sulfides embedded within nitrogen-doped carbon nanoflakes: an efficient and stable electrocatalyst for the oxygen reduction reaction, J. Mater. Chem. A 4 (2016) 11342–11350.

[29] L. Jin, B. Liu, Y. Wu, S. Thanneeru, J. He, Synthesis of mesoporous CoS_2 and $Ni_xCo_{1-x}S_2$ with superior supercapacitive performance a facile solid-phase sulfurization, ACS Appl. Mater. Interfaces 9 (2017) 36837–36848.

[30] X. Li, Q. Li, W. Ye, M. Rui, H. Zeng, Two-dimensional, porous nickel–cobalt sulfide for high-performance asymmetric supercapacitors, ACS Appl. Mater. Interfaces 7 (2015) 19316.

[31] X. Han, K. Tao, D. Wang, L. Han, Design of a porous cobalt sulfide nanosheet array on Ni foam from zeolitic imidazolate frameworks as an advanced electrode for supercapacitors, Nanoscale 10 (2018) 2735–2741.

[32] R.B. Rakhi, N.A. Alhebshi, D.H. Anjum, H.N. Alshareef, Nanostructured cobalt sulfide-on-fiber with tunable morphology as electrodes for asymmetric hybrid supercapacitors, J. Mater. Chem. A 2 (2014) 16190–16198.

[33] S. Kong, Z. Jin, H. Liu, Y. Wang, Morphological effect of graphene nanosheets on ultrathin CoS nanosheets and their applications for high-performance Li-Ion batteries and photocatalysis, J. Phys. Chem. C 118 (2014) 25355–25364.

[34] D. Jiang, Q. Xu, S. Meng, C. Xia, M. Chen, Construction of cobalt sulfide/graphitic carbon nitride hybrid nanosheet composites for high performance supercapacitor electrodes, J. Alloys Compd. 706 (2017) 41–47.

[35] H. Yuan, J. Liu, H. Li, K. Su, X. Liu, Y. Li, D. Shi, Q. Wu, Y. Zhao, Q. Jiao, Rational integration of hierarchical structural $CoS_{1.097}$ nanosheets/reduced graphene oxide nanocomposites with enhanced electrocatalytic performance for triiodide reduction, Carbon 126 (2018) 514–521.

[36] K.Y. Ma, W.J. Zhao, J.P. Cheng, F. Liu, X.B. Zhang, Free-standing α-$Co(OH)_2$/graphene oxide thin films fabricated through delamination and reassembling of acetate anions intercalated α-$Co(OH)_2$ and graphene oxide in water, J. Colloid Interface Sci. 468 (2016) 238–246.

[37] J.P. Cheng, L. Liu, K.Y. Ma, X. Wang, Q.Q. Li, J.S. Wu, F. Liu, Hybrid nanomaterial of α-$Co(OH)_2$ nanosheets and few-layer graphene as an enhanced electrode materials for supercapacitor, J. Colloid Interface Sci. 486 (2017) 344–350.

[38] H. Chen, M.Q. Wang, Y. Yu, H. Liu, S.Y. Lu, S.J. Bao, M. Xu, Assembling hollow cobalt sulfide nanocages array on graphene-like manganese dioxide nanosheets for superior electrochemical capacitors, ACS Appl. Mater. Interfaces 9 (2017) 35040–35047.

[39] R. Xu, H. Chun Zeng, Dimensional control of cobalt-hydroxide-carbonate nanorods and their thermal conversion to one-dimensional arrays of Co_3O_4 nanoparticles, J. Phys. Chem. B 107 (2003) 12643–12649.

[40] K.V. Sankar, Y. Seo, S.C. Lee, S. Liu, A. Kundu, C. Ray, S.C. Jun, Cobalt carbonate hydroxides as advanced battery-type materials for supercapatteries: influence of morphology on performance, Electrochim. Acta 259 (2018) 1037–1044.

[41] Q. Yang, B. Jiang, Q. Xiang, S. Luo, X. Yu, F. Pan, Microstructure evolution and corrosion performance of AZ31 magnesium alloy sheets, Rare Metal Mater. Eng. 45 (2016) 1674–1677.

[42] Q. Wang, X. Liang, D. Yang, D. Zhang, Facile synthesis of novel $CuCo_2S4$ nanospheres for coaxial fiber supercapacitors, RSC Adv. 7 (2017) 29933–29937.

[43] H.B. Li, M.H. Yu, F.X. Wang, P. Liu, Y. Liang, J. Xiao, C.X. Wang, Y.X. Tong, G.W. Yang, Amorphous nickel hydroxide nanospheres with ultrahigh capacitance and energy density as electrochemical pseudocapacitor materials, Nat. Commun. 4 (2013) 1894.

[44] P. Shi, L. Li, L. Hua, Q. Qian, P. Wang, J. Zhou, G. Sun, W. Huang, Design of amorphous manganese oxide@multiwalled carbon nanotube fiber for robust solid-state supercapacitor, ACS Nano 11 (2017) 444–452.

[45] R. Gao, Q. Zhang, F. Soyekwo, C. Lin, R. Lv, Y. Qu, M. Chen, A. Zhu, Q. Liu, Novel amorphous nickel sulfide@CoS double-shelled polyhedral nanocages for supercapacitor electrode materials with superior electrochemical properties, Electrochim. Acta 237 (2017) 94–101.

[46] S.Y. Zhai, L.L. Li, M.G. Wang, A facile synthesis about amorphous CoS_2 combined with first principle analysis for supercapacitor materials, Ionics 23 (2017) 1819–1830.

[47] Q. Chen, D. Cai, H. Zhan, Construction of reduced graphene oxide nanofibers and cobalt sulfide nanocomposite for pseudocapacitors with enhanced performance, J. Alloys Compd. 706 (2017) 126–132.

[48] M. Jin, S.Y. Lu, L. Ma, M.Y. Gan, Y. Lei, X.L. Zhang, G. Fu, P.S. Yang, M.F. Yan, Different distribution of in-situ thin carbon layer in hollow cobalt sulfide nanocages and their application for supercapacitors, J. Power Sources 341 (2017) 294–301.

[49] W. Zhang, C. Ma, J. Fang, J. Cheng, X. Zhang, S. Dong, L. Zhang, Asymmetric electrochemical capacitors with high energy and power density based on graphene/CoAl-LDH and activated carbon electrodes, RSC Adv. 3 (2013) 2483–2490.